Available online at www.sciencedirect.com
SCIENCE DIRECT®
International Journal of Solids and Structures 42 (2005) 3549–3569
INTERNATIONAL JOURNAL OF SOLIDS and STRUCTURES
www.elsevier.com/locate/ijsolstr

A probabilistic approach to the numerical homogenization of irregular solid foams in the finite strain regime

Jörg Hohe [a,*], Wilfried Becker [b]

[a] *Fraunhofer Institut für Werkstoffmechanik, Wöhlerstr. 11, 79108 Freiburg/Brsg., Germany*
[b] *Technische Universität Darmstadt, Institut für Mechanik Hochschulstr. 1, 64289 Darmstadt, Germany*

Received 12 January 2004; received in revised form 14 October 2004
Available online 23 November 2004

Abstract

The present study is concerned with the numerical homogenization of hyperelastic two-dimensional model foams with irregular microstructure under large macroscopic deformation. In contrast to the standard procedure of a single analysis of a large-scale representative volume element where the microstructure is determined by means of a Voronoi tesselation or a similar method, the present study proposes a direct probabilistic approach based on the multiple analysis of small-scale representative volume elements with randomized microstructure. Advantage of this method compared to the standard procedures is the possibility of a proper stochastic assessment of the simulation results. Especially, the scatter which has to be expected in the stress–strain response of the effective material becomes accessible in terms of the standard deviation. In a number of parameter studies it is observed that an increasing microstructural disorder results in a decrease of the effective stiffness of cellular solids due to variations in the underlying microstructural mechanisms of deformation.

Keywords: Foams; Cellular solids; Homogenization; Irregular microstructure; Disorder materials; Stochastic methods

1. Introduction

In modern lightweight construction, solid foams are important materials. Their advantage is their low specific weight due to their high void volume fraction. Another important feature of cellular solids is their high compressibility at an approximately constant stress which makes them a suitable choice for crash absorbing functions. Hence, polymeric foams are widely used in crash and shock absorbing technology

* Corresponding author. Tel.: +49 761 5142 340; fax: +49 761 5142 110.
E-mail address: hohe@iwm.fhg.de (J. Hohe).

0020-7683/$ - see front matter © 2004 Elsevier Ltd. All rights reserved.
doi:10.1016/j.ijsolstr.2004.10.022

as well as in all kinds of packaging and personal protection systems such as safety helmets. Furthermore, solid foams can be used for hybrid structural components performing load-carrying and non-mechanical functions. Examples are filter and catalysator elements or structures with inherent good heat insulation properties.

Solid foams are materials with structural hierarchy (Lakes, 1993), featuring a distinct microstructure. The characteristic intrinsic length is in general much smaller than the characteristic length of the entire structure or component on the macroscopic level. For reasons of numerical efficiency and due to the small ratio of the characteristic intrinsic length scale to the external length scale, the analysis of structures consisting of solid foams is preferrably be performed in terms of effective properties rather than by means of a detailed model of the given microstructure. Therefore, the microstructure is replaced by a homogeneous medium with macroscopically equivalent mechanical properties. The determination of the properties for the homogenized medium can be performed by analytical/numerical or by experimental methods. Advantage of the analytical and numerical methods is that they enable a deeper understanding of the microscopic deformation processes and their specific effects on the macroscopic level of structural hierarchy.

The pioneering work on the analytical homogenization of solid foams has been performed by Gent and Thomas (1963). Further early studies have been published by Dement'ev and Tarakanov (1970) as well as by Patel and Finnie (1970). Due to the increasing interest in lightweight materials, an increasing number of studies on the effective mechanical behavior of foams has been published in the past decade. Among the recent contributions, the work by Christensen (1986), Gibson and Ashby (1997) as well as by Warren and Kraynik (1988) should be mentioned. Compilations of recent work on solid foams can be found in the textbook by Gibson and Ashby (1997) as well as in the review articles by e.g. Ashby (1983) and Gibson (1989) or a review paper by the present authors on the homogenization of two-dimensional cellular structures (Hohe and Becker, 2002).

Most studies on the homogenization of cellular solids are based on regular models with a periodic microstructure. The most common models are the regular hexagonal structure in two-dimensional analyses or the three-dimensional Kelvin foam which both satisfy Kelvin's (1887) optimality criterion for the division of space with minimum partitional area. Nevertheless, real solid foams are amorphous arrangements of pores with different sizes and shapes rather than perfectly periodic structures. Therefore, analyses based on strictly periodic structures might yield inaccurate results. Furthermore, the irregularity of the microstructure yields a significant scatter and variability of the effective properties as it has been observed in a recent experimental study by Ramamurty and Paul (2004). In another recent experimental paper, Blazy et al. (2004) have studied the effect of microstructural disorder on the effective strength of solid foams which is assessed in terms of a Weibull probability density function.

In order to study the effect of different sizes of neighboring pores, Kraynik et al. (1991) have provided an analysis of two-dimensional model foams consisting of a periodic arrangement of a patch of a small number of cells with different sizes. Grenestedt and Bassinet (2000) have contributed a study on the effect of cell wall thickness variations based on the analysis of a periodic Kelvin foam. The most common manner to deal with the problem of irregular microstructures is the analysis of a large scale representative volume element containing a large number of pores where the final geometry of the microstructure is determined by means of a Voronoi technique. Analyses of this type have been provided among others by Chen et al. (1999), Silva et al. (1995) and van der Burg et al. (1997) as well as in recent papers by Fazekas et al. (2002), Huyse and Maes (2001), Roberts and Garboczi (2001) as well as by Zhu et al. (2001) for both, two-dimensional and three-dimensional models.

On the other hand, it has been pointed out by Fortes and Ashby (1999) that a single analysis of a large-scale representative volume element with a stochastic microstructure might still be inaccurate since in some of the previously mentioned studies, artificial anisotropies are still present. Instead, they propose a direct probabilistic approach based on a probability function for cell wall orientations. In an earlier publication, Hall (1993) had proposed a probabilistic model based on the model by Warren and Kraynik (1988) with a

stochastic distribution of the orientation of the Kelvin foam model. A similar model where the effective material is considered as a polycrystal consisting of Kelvin-foam particles with different orientations has later been proposed by Warren and Kraynik (1997) themselves. In a recent paper, Cuitiño and Zheng (2003) have proposed a Taylor averaging technique for hyperelastic foams with different pore sizes.

The present study is concerned with an alternative probabilistic approach. The analysis is based on a homogenization procedure for periodic media which has been developed previously by the present authors for the determination of the effective linear elastic properties of two-dimensional cellular sandwich cores (Hohe and Becker, 2001a,b) and recently has been generalized to the numerical homogenization of periodic two-dimensional model foams at finite deformation (Hohe and Becker, 2003). In the present approach, the microstructure is randomized by a probabilistic determination of the spatial positions of the cell wall intersections within prescribed areas using a random number generator. The mentioned area forms an additional effective material parameter describing the microstructural disorder. The homogenization is performed in multiple numerical experiments which are evaluated by means of stochastic methods. In this context, the expected stress–strain response is obtained in terms of the mean value from the numerical experiments whereas the standard deviation defines the scatter band within which the mechanical response of the foam has to be expected. A similar approach has been employed by Zohdi and Wriggers (2001) in the homogenization of particle reinforced composite materials.

In the following section, the strain energy based concept for homogenization of hyperelastic periodic model foams is outlined. Subsequently, the probabilistic homogenization procedure is derived. In a number of parameter studies, it is observed that an increasing microstructural disorder results not only in an increasing scatter but also in a softening of the effective material with decreasing mean values of the effective stress–strain response. Two-dimensional foam models are used throughout the present study. Nevertheless, the applied principles can easily be generalized to three-dimensional models without any restriction.

2. Homogenization scheme for amorphous solid foams at finite strain

2.1. General concept

Consider a mechanical body Ω according to Fig. 1, consisting of a cellular material. The body is bounded by the external boundary $\partial\Omega = \partial\Omega^{u} \cup \partial\Omega^{t}$. On the boundary $\partial\Omega^{u}$, the components u_i of the displacement vector are prescribed whereas the components $t_i = \sigma_{ij} n_j$ of the traction vector are prescribed on $\partial\Omega^{t}$. The symbols σ_{ij} and n_j denote the components of the Cauchy stress tensor and the outward normal unit vector

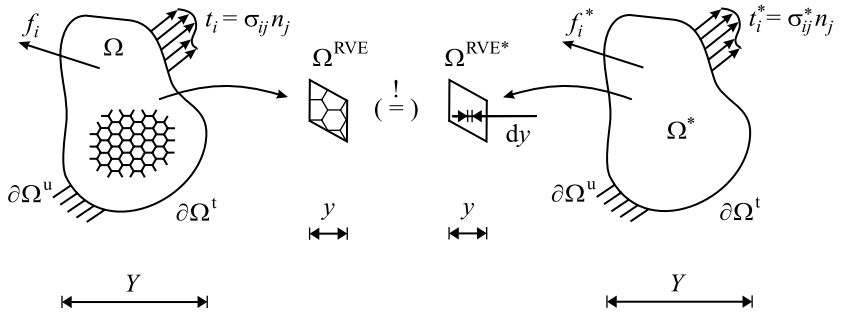

Fig. 1. Concept of the representative volume element.

respectively. In addition to the tractions t_i on $\partial\Omega^{\mathrm{t}}$, the body Ω might be subjected to distributed body forces f_i.

For reasons of numerical efficiency, the body Ω cannot be analyzed by means of a detailed model of the given microstructure. Instead, the body Ω is replaced by a similar body Ω^* which is bounded by the same external boundaries $\partial\Omega^{\mathrm{u}}$ and $\partial\Omega^{\mathrm{t}}$ with the same outward normal unit vector n_i. In contrast to Ω, the replacement body Ω^* is assumed to consist of a homogeneous "effective" material with yet unknown properties. The material constitutive behavior of the replacement body Ω^* has to be determined such that the mechanical response of the two bodies Ω and Ω^* is equivalent on the macroscopic level of structural hierarchy.

If the microstructure of the body Ω does not depend explicitly on the location within Ω, a representative volume element Ω^{RVE} and a similar volume element $\Omega^{\mathrm{RVE}*}$ consisting of the effective medium can be considered for determination of the effective stress–strain response of the replacement body Ω^* (see Fig. 1). In case of a perfectly periodic microstructure, the smallest repeating microstructural volume or a volume consisting of an integer number of these volumes form an appropriate representative volume element. For random microstructures, the representative volume element has to be chosen such that it containes a sufficient number of the different constituents in order to be statistically representative for the microstructure of Ω. The constitutive behavior of the volume element $\Omega^{\mathrm{RVE}*}$ has to be chosen such that the mechanical behavior of both volume elements is macroscopically equivalent. In general, the characteristic dimension y of the representative volume element is much smaller than the characteristic dimension Y of the entire body but larger than the infinitesimal length scale $\mathrm{d}y$ ($Y \gg y \gg \mathrm{d}y$).

Similar as in a preceding article by the present authors (Hohe and Becker, 2003), the mechanical behavior of the two volume elements Ω^{RVE} and $\Omega^{\mathrm{RVE}*}$ is assumed to be macroscopically equivalent, if the average strain energy in both volume elements is equal, provided that both volume elements are subjected to a macroscopically equivalent deformation. For the strain energy density w in both volume elements, the equivalence condition

$$\bar{w} = \frac{1}{V^{\mathrm{RVE}}} \int_{\Omega^{\mathrm{RVE}}} w \, \mathrm{d}V = \frac{1}{V^{\mathrm{RVE}}} \int_{\Omega^{\mathrm{RVE}*}} w^* \, \mathrm{d}V = \bar{w}^* \tag{1}$$

has to be satisfied, where V^{RVE} is the volume of both volume elements. In Eq. (1) as well as in all subsequent equations, overbars denote volume averages whereas symbols marked with an asterisk denote quantities related to the effective medium. The deformation of both volume elements is defined to be macroscopically equivalent, if the volume average of the components F_{ij} of the deformation gradient is equal for both volume elements:

$$\overline{F}_{ij} = \frac{1}{V^{\mathrm{RVE}}} \int_{\Omega^{\mathrm{RVE}}} F_{ij} \, \mathrm{d}V = \frac{1}{V^{\mathrm{RVE}}} \int_{\Omega^{\mathrm{RVE}*}} F^*_{ij} \, \mathrm{d}V = \overline{F}^*_{ij} \tag{2}$$

In the case of hyperelastic material behavior, the macroscopic stress and strain components are related to the stress and strain components on the effective level by means of their definitions

$$\bar{\gamma}_{ij} = \frac{1}{2}(\overline{F}_{ki}\overline{F}_{kj} - \delta_{ij}) \tag{3}$$

$$\bar{\tau}_{ij} = \frac{\partial \bar{w}}{\partial \bar{\gamma}_{ij}} \approx \frac{\Delta \bar{w}}{\Delta \bar{\gamma}_{ij}} \tag{4}$$

where $\bar{\gamma}_{ij}$ and $\bar{\tau}_{ij}$ are the components of the effective Green-Lagrange strain tensor and the second Piola-Kirchhoff stress tensor respectively.

The application of the homogenization scheme defined by Eqs. (1)–(4) for determination of the effective stress–strain response of hyperelastic cellular solids requires the following four steps:

- identification of an appropriate representative volume element,
- deformation of the representative volume element consisting of the given microstructure according to the desired effective strain state $\bar{\gamma}_{ij}$,
- computation of the strain energy for the given strain state and the corresponding partial derivatives,
- determination of the effective stress components $\bar{\tau}_{ij}$ using Eq. (4).

Details are given in the following sections. Within this scheme, the structural analysis of the representative volume element can be performed by means of any suitable analytical or numerical method. The present results have been obtained by means of finite element analyses.

2.2. Perfectly periodic microstructures

Prior to the application to random, irregular microstructures, the application of the homogenization procedure defined in Section 2.1 to perfectly periodic microstructures is briefly outlined. The perfectly periodic model forms the base for the enhanced model for irregular microstructures presented subsequently in Section 2.3. All subsequent derivations are related to two-dimensional microstructures for reasons of numerical efficiency and an easier visualization. Nevertheless, all principles employed in this simplified analysis can be applied to a fully three-dimensional analysis in the same manner without any restrictions.

An appropriate representative volume element for periodic two-dimensional cellular media with general geometry and topology is presented in Fig. 2. Note that the microstructure in this figure—although it already includes some irregularity—is a strictly periodic array formed by a repeating arrangement of the three highlighted cells. For all types of periodic two-dimensional microstructures, similar parallelogram-shaped representative volume elements can be identified. The representative volume element is defined by two vectors $\boldsymbol{a}$ and $\boldsymbol{b}$ which originate from any arbitrary point of the microstructure and point to the next corresponding points of the periodic arrangement in two independent directions (see Fig. 2).

Similar as in a previous study (Hohe and Becker, 2003), the cell walls of the representative volume element are meshed by a single layer of standard four-node shell elements in an upright orientation. The element is based on an enhanced strain formulation in conjunction with a full integration scheme. All displacements normal to the x_1–x_2-plane are constrained in order to ensure proper plane strain conditions. Along the external boundaries of the representative volume element, periodic boundary conditions are applied. These conditions require that the displacements of the corresponding opposite boundaries are interrelated by

$$\frac{\partial u_i^+}{\partial s} = \frac{\partial u_i^-}{\partial s} \tag{5}$$

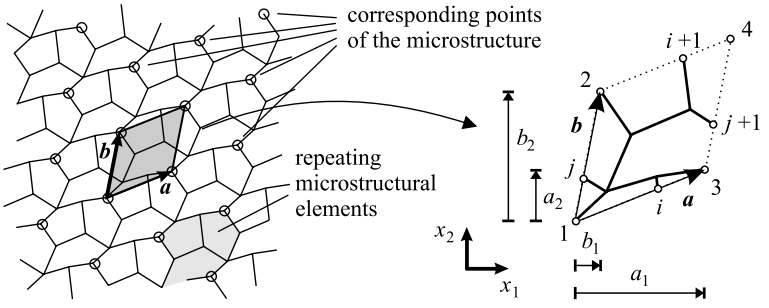

Fig. 2. Representative volume element for general two-dimensional cellular structures.

where s is a local coordinate pointing along the respective surface whereas u_i^+ and u_i^- are the displacements of the upper and lower surface respectively. By virtue of Eq. (5) it is ensured that neighboring volume elements, which set up the entire structure, fit at their joint boundaries even in the deformed configuration. In the discretized form, the periodic boundary conditions along the external surfaces parallel to the vector $\boldsymbol{a}$ take the form

$$u_k^{(i+1)} = u_k^{(i)} + u_k^{(2)} - u_k^{(1)} \tag{6}$$

$$u_k^{(4)} = u_k^{(3)} + u_k^{(2)} - u_k^{(1)} \tag{7}$$

$$\varphi_3^{(i+1)} = \varphi_3^{(i)} \tag{8}$$

$$\varphi_3^{(4)} = \varphi_3^{(3)} \tag{9}$$

where $u_k^{(i)}$ and $\varphi_k^{(i)}$ denote the displacement and the rotation of node no. i with respect to the x_k-axis respectively. In a similar manner, the conditions

$$u_k^{(j+1)} = u_k^{(j)} + u_k^{(2)} - u_k^{(1)} \tag{10}$$

$$\varphi_3^{(j+1)} = \varphi_3^{(j)} \tag{11}$$

hold for the nodes on the surfaces parallel to the vector $\boldsymbol{b}$.

The finite element model is loaded by prescribed displacements of the corner nodes no. 1, 2 and 3 according to the prescribed macroscopic strain state $\bar{\gamma}_{ij}$. Expressions for the displacements of the corner nodes in terms of the effective strain state can be derived from the two-dimensional equivalent to the kinematic equivalence condition (2). Replacing the deformation gradient F_{ij}^* for the given microstructure by its definition in terms of the displacement gradient $u_{i,j}^*$ and transformation of the area integral into a boundary integral using Green's theorem yields

$$\overline{F}_{ij} = \overline{F}_{ij}^* = \frac{1}{A^{\mathrm{RVE}}} \int_{\partial A^{\mathrm{RVE}}} u_i^* n_j \, \mathrm{d}s + \delta_{ij} \tag{12}$$

where A^{RVE} is the area of the representative volume element within the x_1–x_2-plane, $\partial A^{\mathrm{RVE}}$ is its external boundary and s is a coordinate along $\partial A^{\mathrm{RVE}}$. If the displacements between neighboring nodes on the external boundaries are interpolated and the periodicity requirements (5) are considered, the integral in Eq. (12) can be evaluated, resulting in

$$\overline{F}_{11} = \frac{(a_1 + u_1^{(3)} - u_1^{(1)})b_2 - (b_1 + u_1^{(2)} - u_1^{(1)})a_2}{a_1 b_2 - b_1 a_2} \tag{13}$$

$$\overline{F}_{12} = \frac{(u_1^{(2)} - u_1^{(1)})a_1 - (u_1^{(3)} - u_1^{(1)})b_1}{a_1 b_2 - b_1 a_2} \tag{14}$$

$$\overline{F}_{21} = \frac{(u_2^{(3)} - u_2^{(1)})b_2 - (u_2^{(2)} - u_2^{(1)})a_2}{a_1 b_2 - b_1 a_2} \tag{15}$$

$$\overline{F}_{22} = \frac{(b_2 + u_2^{(2)} - u_2^{(1)})a_1 - (a_2 + u_2^{(3)} - u_2^{(1)})b_1}{a_1 b_2 - b_1 a_2} \tag{16}$$

where a_i and b_i are the components of the vectors $\boldsymbol{a}$ and $\boldsymbol{b}$ defining the representative volume element (see Fig. 2). Substituting Eqs. (13)–(16) into the definition (3) of the macroscopic strain $\bar{\gamma}_{ij}$ yields a system of

three nonlinear equations for the six unknown displacement components $u_i^{(j)}$ of the corner nodes no. 1, 2 and 3. Together with three conditions for suppression of translatoric and rotatory rigid body motions of the representative volume element, a complete system of equations for the displacements of the corner nodes in terms of the prescribed effective strain state $\bar{\gamma}_{ij}$ is obtained. The system is solved by means of Newton's method.

From the solution in conjunction with the discretized periodicity conditions (6)–(11), the displacements of all four corner nodes of the representative volume element are prescribed directly in terms of the effective strain state whereas the displacements of the nodes between the corner nodes on the upper surfaces are prescribed in terms of the prescribed effective strain state and the displacements of the corresponding nodes on the lower surfaces which remain movable. The finite element analysis is performed for the desired effective strain state $\bar{\gamma}_{ij}$ and for neighboring effective strain states $\bar{\gamma}_{ij} + \Delta\bar{\gamma}_{ij}$. Subsequently, the corresponding effective stress components $\bar{\tau}_{ij}$ are obtained from Eq. (4).

No cell wall interaction due to cell wall contact is included in the finite element model. Instead, the analysis is stopped, if cell wall contact occurs at rather large effective strain levels $\bar{\gamma}_{ij}$. Nevertheless, it has been observed in a previous paper using a similar finite element model (Hohe and Becker, 2003) that cell wall contact for two-dimensional model foams is a feature, which occurs only at rather large effective strain levels. Hence, the restriction introduced by the missing contact formulation is limited to rather large compressive strain levels close to the point where self-interpenetration of the representative volume element would occur.

2.3. Enhanced probabilistic model for irregular cellular microstructures

Solid foams are amorphous media consisting of cell walls and pores with different shapes and sizes rather than being perfectly periodic arrangements of cells with equal size and shape as assumed in Section 2.2. Therefore, the developed procedure has to be enhanced for a more realistic modeling of solid foams. A simple possibility for an enhancement is the analysis of a large-scale representative volume element with a random microstructure as it is done in most studies in literature (e.g. Silva et al., 1995; van der Burg et al., 1997 among others). On the other hand, as it has been pointed out by Fortes and Ashby (1999), rather large representative volume elements might be needed in order to avoid the development of artificial numerical anisotropies. Instead, direct probabilistic approaches are more desirable.

Therefore, the microstructure of the representative volume element presented in Fig. 2 is randomized by a random determination of the spatial positions of the cell wall intersections within prescribed areas of dimension $2\Delta x_1 \times 2\Delta x_2$ around the respective position in case of a "perfect" microstructure with regular cell shape (see Fig. 3). Thus, the topology of the microstructure is prescribed (e.g. regular hexagonal)

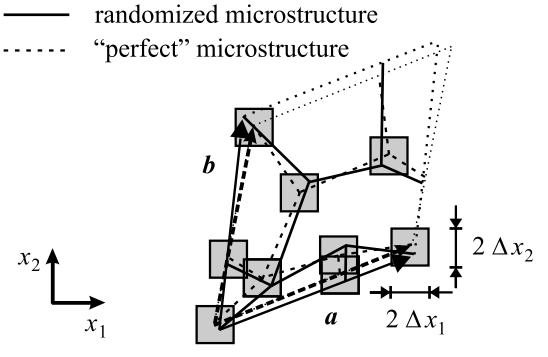

Fig. 3. Randomized cellular structure.

whereas the geometry of the individual cells varies randomly. The degree of possible microstructural disorder is controlled by the parameters Δx_1 and Δx_2 which form additional effective material parameters. For any kind of given cellular solid, the degree of microstructural disorder can easily be determined from micrographic observations. In most cases, especially for isotropic microstructures $\Delta x_1 = \Delta x_2$ will be an appropriate assumption. Note that the position of the nodes on the upper surfaces of the representative volume element except the corner nodes no. 2 and 3 is not independent for reasons of periodicity of the randomized microstructure (see Figs. 2 and 3).

Since interaction effects between neighboring pores of different size and shape can be important features in the effective stress–strain response of irregular solid foams, the choice of a representative volume element as the smallest possible repeating assembly according to Fig. 2 of the periodic reference microstructure is no longer appropriate. Instead, patches consisting of small integer numbers of the smallest possible repeating assembly in all spatial directions are used as a representative volume element. In this context, the required number of repeating assemblies is determined in a study of convergence presented in Section 3.2. With respect to the external surfaces of the representative volume element, the periodic boundary conditions (6)–(11) are retained in order not to overconstrain the microstructure.

For each considered effective strain state $\bar{\gamma}_{ij}$, the analysis is performed multiple times with an independent random determination of the microstructural geometry for each of the numerical experiments. Subsequently, the effective stress is defined in terms of the mean value

$$\bar{\tau}^{\mathrm{a}}_{ij} = \frac{1}{n}\sum_{k=1}^{n} \bar{\tau}^{(k)}_{ij} \tag{17}$$

where $\bar{\tau}^{(k)}_{ij}$ is the effective stress obtained for the individual numerical experiments and n is the total number of numerical experiments. The scatter which has to be expected in the effective stress–strain relation for a cellular solid with a known degree of microstructural disorder can be assessed in terms of the standard deviation

$$\bar{\tau}^{\mathrm{s}}_{ij} = \left(\frac{1}{n-1}\sum_{k=1}^{n} \left(\bar{\tau}^{\mathrm{a}}_{ij} - \bar{\tau}^{(k)}_{ij} \right)^2 \right)^{\frac{1}{2}}. \tag{18}$$

The main advantage of the probabilistic approach compared to the standard approaches based on the single analysis of a large-scale representative volume element available in the literature is that it addresses both, the mean values of the effective stresses (or the effective stiffness if used in conjunction with linear elasticity) and the corresponding scatter bands. Due to its simple formulation, the scheme provides an efficient and easy-to-use procedure for the numerical homogenization of random microstructures if it is used in conjunction with parameterized finite element modeling and automatic mesh generation.

3. Results

3.1. Periodic reference foam model

As a two-dimensional periodic reference foam model, the case of a regular hexagonal cellular structure is employed. This kind of microstructure satisfies both, Kelvin's (1887) optimality criterion as well as Christensen's 1987 isotropy criterion for small deformations and therefore constitutes the "best" possible periodic two-dimensional foam model. The microstructure and an appropriate representative volume element consisting of the smallest possible repeating microstructural assembly are presented in Fig. 4. A constant cell wall angle of $\psi = 120°$ is assumed for all cell wall intersections. All struts in the model are of equal

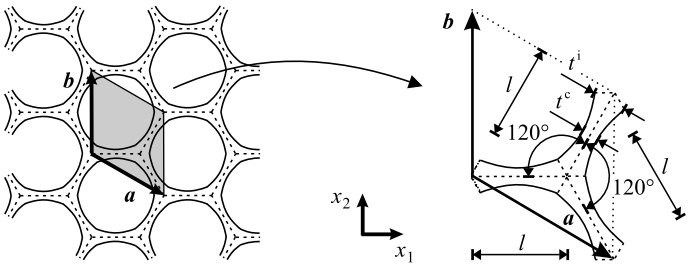

Fig. 4. Hexagonal two-dimensional model foam (periodic microstructure).

length l. For a realistic modeling of the foam geometry, a quadratic material or thickness distribution along the cell walls is assumed which is defined by the cell wall thickness t^{c} at the center of the struts and the strut thickness t^{i} at the cell wall intersections. The strut thicknesses t^{c} and t^{i} respectively are assumed to be the same for all struts in the model. The actual values of the strut thicknesses are determined such that a prescribed relative density $\bar{\rho}$ is obtained.

For the cell walls a compressible Ogden (1984) type hyperelastic material model is assumed. The strain energy potential is given by

$$w = \sum_{k=1}^{n} \frac{\mu_{(k)}}{\alpha_{(k)}} \left(\left(\lambda_1^{\mathrm{dev}}\right)^{\alpha_{(k)}} + \left(\lambda_2^{\mathrm{dev}}\right)^{\alpha_{(k)}} + \left(\lambda_3^{\mathrm{dev}}\right)^{\alpha_{(k)}} - 3 \right) + \sum_{k=1}^{n} \kappa_{(k)} (J-1)^{2k} \tag{19}$$

with

$$\lambda_k^{\mathrm{dev}} = J^{-\frac{1}{3}} \lambda_k$$

where λ_k are the principal values of the deformation gradient whereas J denotes the corresponding Jacobian. Within the Ogden material model (19), the quantities n and $\alpha_{(k)}$ as well as the generalized shear and compression moduli $\mu_{(k)}$ and $\kappa_{(k)}$ respectively are material constants ($k = 1, \ldots, n$). Throughout the present study, the material parameters are assumed as $n = 2$ with $\alpha_1 = 1.5$, $\mu_1 = 0.7\,\mathrm{GPa}$ and $\kappa_1 = 0.4\,\mathrm{GPa}$ as well as $\alpha_2 = 3$, $\mu_2 = 0.5\,\mathrm{GPa}$ and $\kappa_2 = 0$. The material response defined by these parameters is within the range of typical polymeric materials.

In the non-probabilistic analysis of the reference model foam, a representative volume element according to Fig. 4 consisting of the smallest possible repeating microstructural assembly is considered. For randomized microstructures, patches consisting of $m \times m$ repeating elements (where m is a small integer number) are assumed as representative volume elements. In order to regularize the mechanical response in occurrence of bifurcation points, some small geometrical imperfections are applied.

3.2. Convergence

Before the concept for numerical homogenization of irregular solid foams defined in Section 2 can be applied to any kind of specific problem, the convergence of the proposed scheme has to be investigated. The study of convergence has to be performed with respect to both, the number n of numerical experiments as well as the number m of the repeating microstructural assemblies in the representative volume element. Three different effective strain states involving all basic modes of deformation are considered:

- uniaxial tensile deformation within the x_1-direction with $\bar{\gamma}_{11} = 0.2$ and $\bar{\gamma}_{22} = \bar{\gamma}_{12} = 0$,
- uniaxial compressive deformation within the x_1-direction with $\bar{\gamma}_{11} = -0.2$ and $\bar{\gamma}_{22} = \bar{\gamma}_{12} = 0$ as well as
- pure shear deformation within the x_1–x_2-plane with $\bar{\gamma}_{11} = \bar{\gamma}_{22} = 0$ and $\bar{\gamma}_{12} = 0.2$.

The results for the study of convergence regarding the number n of numerical experiments are presented in Fig. 5. In this study, the areas for probabilistic determination of the spatial position of the cell wall intersections (see Fig. 3) are assumed to be equal for all cell wall intersections with an edge length of $\Delta x_1 = \Delta x_2 = 0.2l$. The cell walls are assumed to be of uniform thickness with $t^c = t^i$. The assumed relative density of the foam is $\bar{\rho} = 5\%$. A patch of 2×2 repeating microstructural cell wall assemblies according to Fig. 3 forms the underlying representative volume element. In the first column of Fig. 5, the mean values $\bar{\tau}^a_{11}$, $\bar{\tau}^a_{22}$ and $\bar{\tau}^{12}_{12}$ of the three effective in-plane stress components for all three macroscopic reference strain states are presented. The stress components are plotted depending on the number n of numerical experiments included in the stochastic evaluation according to Eq. (17). In the second column, the corresponding standard deviations are given. The numerical experiments are included in the order as they were computed. No ranking or other re-arrangement is performed.

For the case of the uniaxial tensile deformation, nearly constant mean values $\bar{\tau}^a_{ij}$ are obtained throughout the considered range for the number n of numerical experiments except some slight initial scatter for small n. The initial scatter is slightly more distinct in case of the uniaxial compressive deformation. Nevertheless,

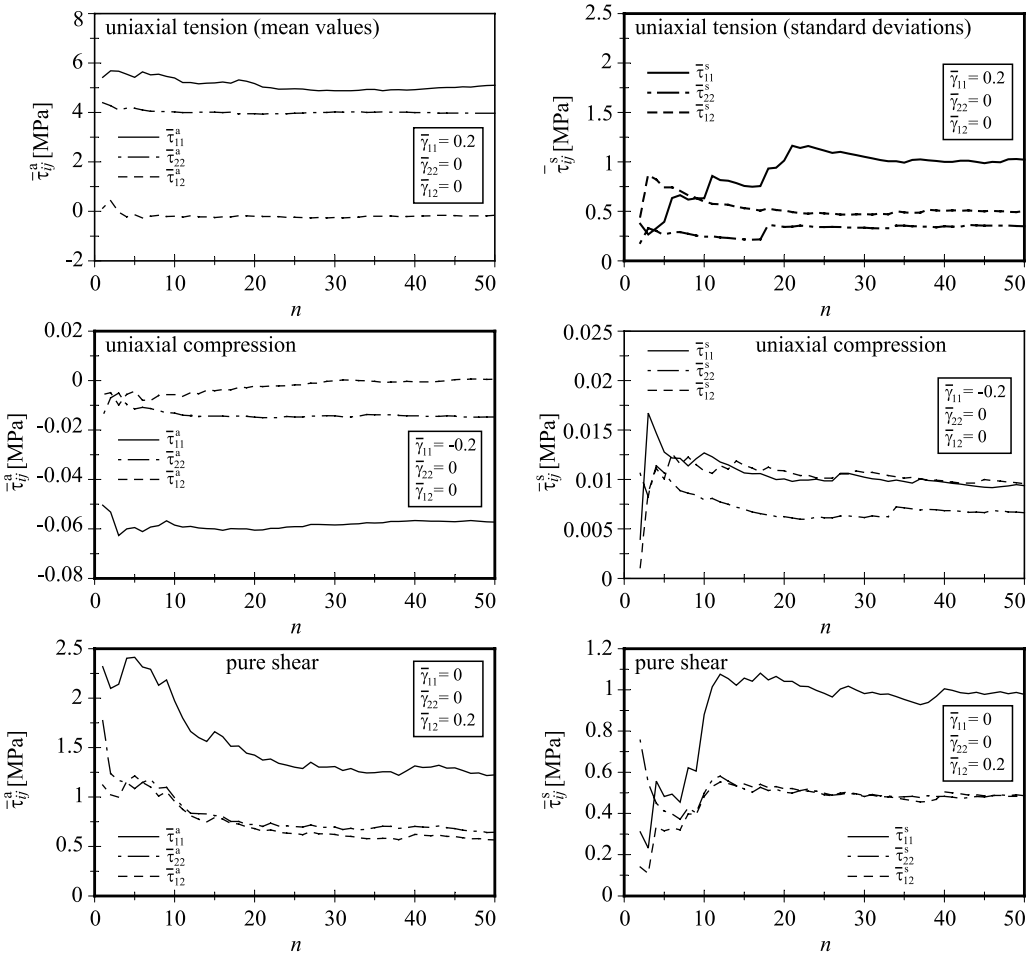

Fig. 5. Study of convergence—number of numerical experiments.

even for this load case, the mean values become more or less stable for $n > 30$. In the pure shear deformation case the effect occurs that the first ten numerical experiments yield effective stress results which are close to each other but far from the final mean values. Therefore, an initial range with high average stresses with a distinct scatter due to the still small number of numerical experiments is followed by a successive degradation towards their final mean values at lower levels. The convergence of the corresponding standard deviations $\bar{\tau}^{s}_{ij}$ in general proves to be slower than the convergence of the stress mean values. Nevertheless, for $n > 30$, no severe scatter is observed in any of the considered macroscopic states of deformation. Note that in all cases, the actual shape of the plotted curves and their development towards their final stable values strongly depends on the order of the numerical experiments. Therefore, the occurrence of an extreme case of the cellular microstructure can have different effects whether it occurs in one of the early or in one of the later numerical experiments. In order to avoid problems caused by the possible occurrence of extreme microstructures, all subsequent analyses are based on 50 numerical experiments. For $n = 50$, stable results can be expected while the analysis still can be performed in a numerically efficient manner.

In a second study of convergence, the effect of the number m of repeating microstructural assemblies forming the representative volume element is investigated. The study is based on the same type of microstructure as the first study of convergence. In contrast to this study, the number of numerical experiments is kept constant at $n = 50$ whereas the number m of repeating microstructural assemblies according to Fig. 4 is varied. Again, the basic load cases of uniaxial tensile deformation with $\bar{\gamma}_{11} = 0.2$, uniaxial compressive deformation with $\bar{\gamma}_{11} = -0.2$ and pure shear deformation with $\bar{\gamma}_{12} = 0.2$ are considered. The results for the stress mean values $\bar{\tau}_{ij}$ are presented in Fig. 6.

It is observed that for the case of uniaxial tensile deformation, the number m of repeating microstructural assemblies in the representative volume element has only minor effects. For both, the case of uniaxial

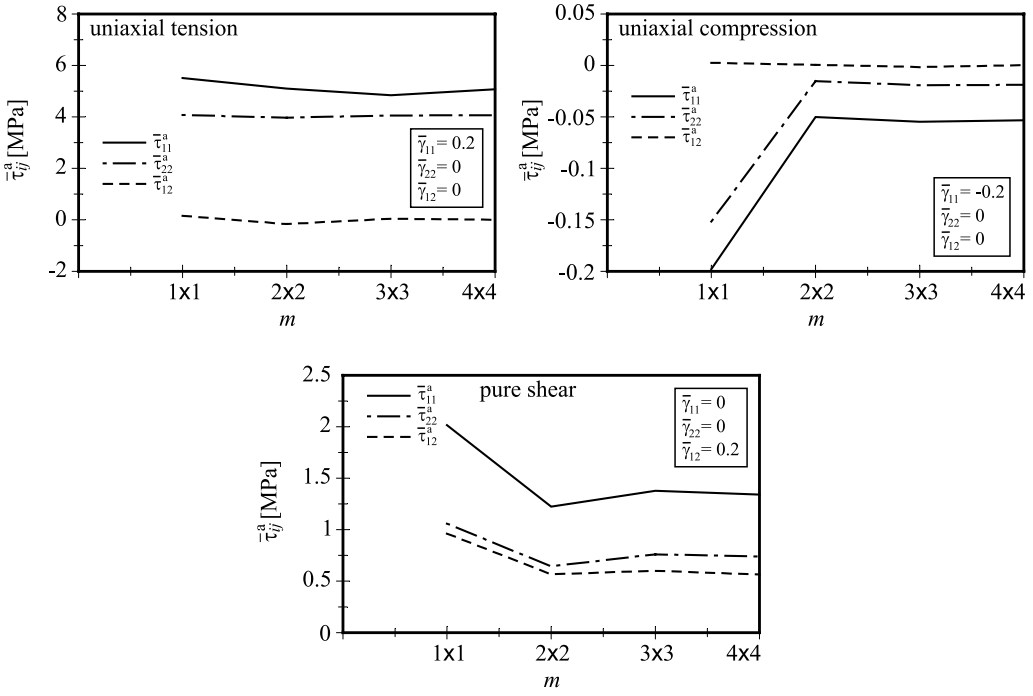

Fig. 6. Study of convergence—size of representative volume element.

compressive deformation and pure shear deformation, a distinct decrease is obtained in the level of the mean values of effective stresses between $m = 1$ and $m = 2$. For larger numbers m, only minor variations are observed. For the case of uniaxial compressive deformation, the decrease in the stress levels is not only of stochastic nature. For the case of a perfectly periodic hexagonal structure, the microstructure would be in a postbuckling state at the prescribed effective stress level $\bar{\gamma}_{11} = -0.2$. Since all of the lower eigenmodes for regular hexagonal structures achieve periodicity only with respect to two neighboring repeating cells (Gibson and Ashby, 1997; Hohe and Becker, 2003), the patch consisting of 2×2 repeating microstructural assemblies results in significantly lower effective stresses than its 1×1 counterpart which deforms according to a higher-order eigenmode. Similar microstructural modes of deformation develop for irregular microstructures resulting in a similar effect on the effective stress levels.

In all three considered modes of deformation, the results for the stress mean values for $m = 2$ and $m = 4$ respectively are nearly identical. Therefore, $m = 2$ is assumed to be sufficiently high. All subsequent analyses are based on this value.

3.3. Effect of the microstructural irregularity

As a first parameter study, the effect of the microstructural cell irregularity on the effective stress–strain response is studied in more detail. In Fig. 7, the effective stress–strain curves are presented for four different degrees of cell irregularity characterized by the ratios $\Delta x_i/l$ of the edge lengths of the areas permitted for random determination of the spatial positions of the cell wall intersections to the nominal cell wall lengths l of the underlying regular hexagonal reference structure. The edge lengths Δx_1 and Δx_2 are assumed to be equal in the present example, as well as in all subsequent analyses. Note that the largest degree of cell irregularity considered ($\Delta x_i/l = 0.3$) might result in microstructures where the area of individual hexagonal cells is between 39% and 189% of the cell area for the underlying regular hexagonal microstructure resulting in a ratio of the maximum possible cell area to the minimum possible cell area of about 4.8. Thus, the case $\Delta x_i/l = 0.3$ constitutes a two-dimensional cellular solid with a rather high degree of microstructural irregularity. The other extremum case of microstructural irregularity considered in Fig. 7 corresponds to vanishing areas for random determination of the spatial positions of the cell wall intersections ($\Delta x_i/l = 0$). Here, the case of the perfectly regular hexagonal microstructure is recovered, which is employed in most of the previous deterministic approaches.

In all cases, a constant cell wall thickness with $t^c = t^i$ is assumed. The cell wall thickness is chosen according to a relative density of 5%. Again, three different types of macroscopic deformation are considered:

- uniaxial tensile deformation within the x_1-direction with $\bar{\gamma}_{11} \in [0, 1]$,
- uniaxial compressive deformation within the x_1-direction with $\bar{\gamma}_{11} \in [-0.4, 0]$ and
- pure shear deformation within the x_1–x_2-plane with $\bar{\gamma}_{12} \in [0, 0.4]$.

Note that due to the nonlinear nature of the Green-Lagrange strain tensor, the cases $\bar{\gamma}_{11} = -0.5$ and $\bar{\gamma}_{12} = \pm 0.5$ form the limit cases with 100% engineering strain where self-penetration of the representative volume element would occur.

In the plots in the first line of Fig. 7, the effective stress mean values $\bar{\tau}^a_{11}$ acting within the direction of macroscopic deformation as well as the macroscopic net stresses $\bar{\tau}^a_{22}$ are presented. The corresponding standard deviations $\bar{\tau}^s_{ij}$ are presented as thin lines of the same type as the corresponding mean values. Regarding the mean values of the effective stresses $\bar{\tau}^a_{11}$ within the loading direction, almost no effect of the microstructural irregularity is observed. Nevertheless, increasing degrees $\Delta x_i/l$ of microstructural disorder result in increasing standard deviations $\bar{\tau}^s_{11}$ indicating an increasing width of the scatter band within which the macroscopic stress has to be expected.

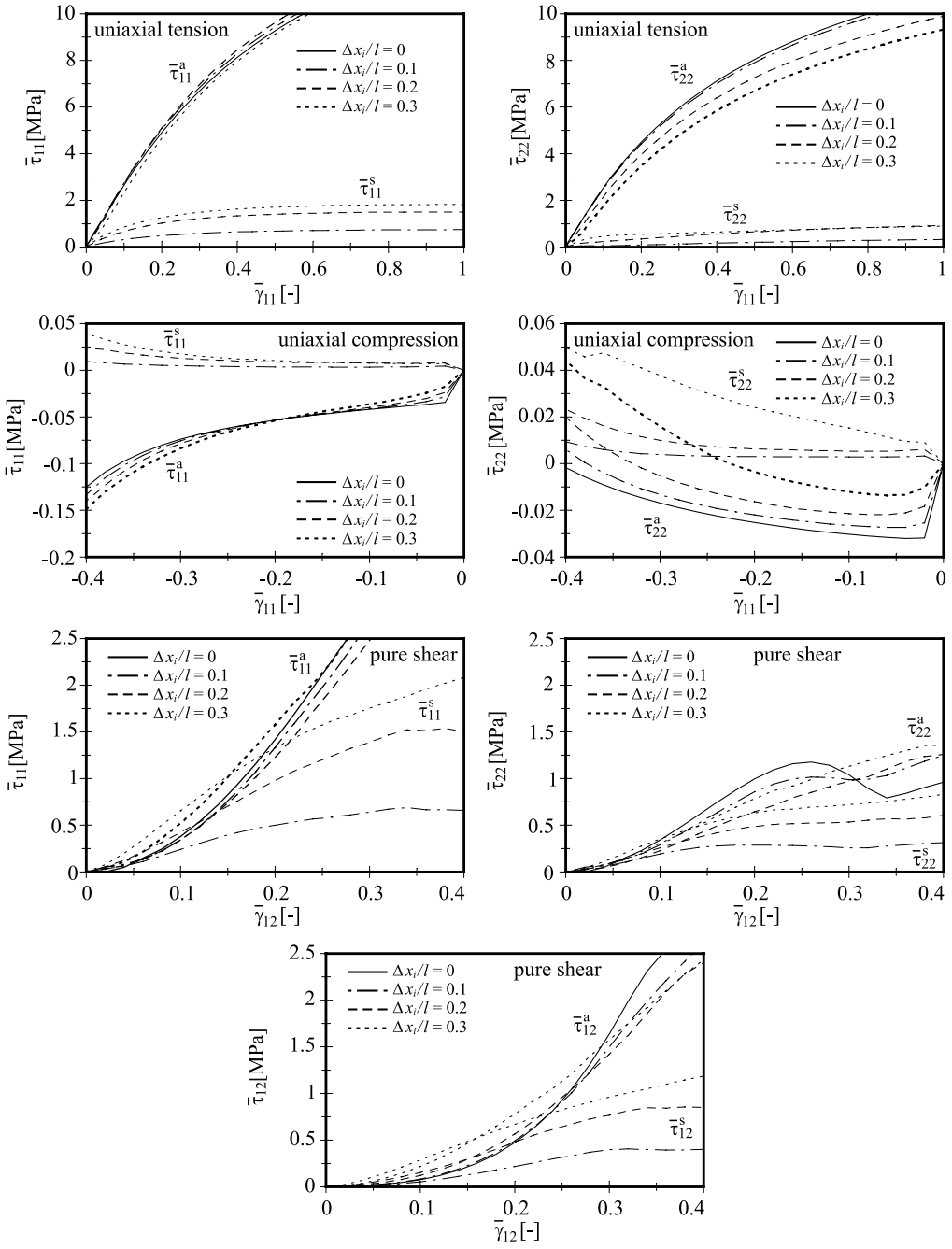

Fig. 7. Effect of the cell irregularity.

In their experimental study on disorder effects in the macroscopic response of closed-cell metallic foams, Ramamurty and Paul (2004) have observed a variance E^s/E^a in the effective Young's moduli of up to 16%. The results are not directly comparable with the present results since Ramamurty and Paul are concerned

with linear elasticity occurring at small deformation of elastic-plastic metal foams whereas the present study is concerned with the nonlinear elastic response of polymeric foams. Nevertheless, the variance observed by Ramamurty and Paul (2004) in the effective Young's moduli is approximately the same as the effective stress variance observed in Fig. 7 for the model foam with a moderate degree of microstructural disorder ($\Delta x_i/l = 0.2$) at a moderately large effective strain level of $\bar{\gamma}_{11} = 0.1$. The fact that the variances observed experimentally and determined numerically are in the same order of magnitude gives evidence for the strong capabilities of the present approach in the modelling of cellular solids with randomly disordered microstructure.

Regarding the net stress mean values $\bar{\tau}^{a}_{22}$ perpendicular to the macroscopic loading direction, an increasing degree of microstructural disorder results in a softening of the model foam on the macroscopic level of structural hierarchy. In this context, the effect that the generalized effective Poisson's ratio $\bar{\nu}_{12} = \bar{\tau}^{a}_{22}/\bar{\tau}^{a}_{11}$ is deformation-dependent, which already occurs in the case of perfectly regular hexagonal microstructures (see Hohe and Becker, 2003), becomes more severe with increasing microstructural disorder. For small deformations, an effective Poisson's ratio of $\bar{\nu}_{12} = 1$ is obtained as it is known from small strain analyses (see e.g. Gibson and Ashby, 1997) resulting in equal stress mean values $\bar{\tau}^{a}_{11}$ and $\bar{\tau}^{a}_{22}$ within and perpendicular to the macroscopic loading direction if $\bar{\gamma} \to 0$. For increasing macroscopic strain levels $\bar{\gamma}_{11}$ and increasing degrees $\Delta x_i/l$ of microstructural disorder, increasing differences between both stress components develop. The mean value of the effective shear stress $\bar{\tau}^{a}_{12}$ vanishes throughout the considered range of effective strains and is therefore not presented explicitly. Nevertheless, it should be noted that even if the mean values of the effective shear stresses vanish, increasing standard deviations $\bar{\tau}^{s}_{12}$ indicate an increasing scatter band width with increasing microstructural disorder. Therefore, for high degrees of microstructural disorder, some shear stresses might develop even in the case of pure stretching deformation on the macroscopic level.

In the second line of plots in Fig. 7, the normal stresses $\bar{\tau}^{a}_{11}$ and $\bar{\tau}^{a}_{22}$ acting within and perpendicular to the macroscopic loading direction are presented for the case of uniaxial compressive deformation within the x_1-direction. The effective shear stresses $\bar{\tau}^{a}_{12}$ are vanishing. Therefore, no shear stress plot is included. In the current effective deformation mode, a microstructural instability phenomenon is encountered for the case of a perfectly regular microstructure at small effective strain levels. A kink in the macroscopic stress–strain curve separates the prebuckling range with a steep increase of the effective stress levels with increasing compressive strain levels from the postbuckling range with a plateau region followed by a moderate secondary increase of the normal stress level $-\bar{\tau}^{a}_{11}$ at high levels of the prescribed effective strain ($\bar{\gamma}_{11} < 0.3$). In the postbuckling range, only the stable branch of the stress–strain curve is presented. For the imperfect irregular microstructures with $\Delta x_1 > 0$, no buckling in the Eulerian sense is present. Instead of the kink in the effective stress–strain curve, a soft transition between the initial steep curve and the plateau region is achieved. At high levels of the prescribed macroscopic effective strain $\bar{\gamma}_{11}$, an increasing degree $\Delta x_i/l$ of microstructural disorder results in an increase in the mean value of the macroscopic normal stress level $-\bar{\tau}^{a}_{11}$. In this context, the plateau region in the macroscopic stress–strain response becomes less distinct with increasing degrees of microstructural disorder where the effective stress–strain response develops towards a curve with only moderate changes in the first gradient.

More distinct effects of the degree $\Delta x_1/l$ of microstructural disorder are observed in terms of the net stress $\bar{\tau}_{22}$ acting perpendicular to the direction of the applied effective strain $\bar{\gamma}_{11}$. Here, a deformation induced negative generalized Poisson's ratio occurs on the effective level for $\bar{\gamma}_{11} \approx -0.4$ (Hohe and Becker, 2003). For increasing degrees of microstructural disorder, the point of the first occurrence of a negative effective Poisson's ratio is shifted towards lower levels of effective strain $\bar{\gamma}_{11}$. Especially for the largest degree of microstructural disorder ($\Delta x_i/l = 0.3$), a large scatter band width occurs with a standard deviation $\bar{\tau}^{s}_{22}$ which is in the same order of magnitude as the corresponding mean value $\bar{\tau}^{a}_{22}$. For smaller degrees of microstructural disorder, the scatter band width is in general smaller. Nevertheless, even in theses cases, a distinct increase in the standard deviation $\bar{\tau}^{s}_{22}$ and therefore in the scatter band width occurs, if the occurrence of a negative effective Poisson's ratio with a positive mean value $\bar{\tau}^{a}_{22}$ of the net stress is approached or exceeded.

For the case of the largest considered degree of microstructural disorder ($\Delta x_i/l = 0.3$) at a high effective strain level ($\bar{\gamma}_{11} \approx -0.36$), a kink is observed in the curves for both the mean stress $\bar{\tau}^{a}_{22}$ and the standard deviation $\bar{\tau}^{s}_{11}$. The reason for this kink is that especially for microstructures with a large degree of disorder, extreme microstructural geometries might occur for which the numerical simulation breaks down at large effective deformations. In this event, the stochastic evaluation of the numerical experiments at higher effective strain levels is continued with the remaining numerical experiments. On the other hand, the sudden change in the underlying database causes an increase in the weight factors for the remaining numerical experiments from 1/50 to 1/49 (and maybe more) since the following data points are computed with less than $n = 50$ numerical experiments. The shrinking of the database results in the observed discontinuities in the gradients of the macroscopic stress strain curves.

In the bottom three plots in Fig. 7, the in-plane stress components $\bar{\tau}_{11}$, $\bar{\tau}_{22}$ and $\bar{\tau}_{12}$ in case of a pure shear deformation $\bar{\gamma}_{12}$ on the macroscopic level are presented. In contrast to small strain analyses, where no coupling of normal and shear deformation occurs (see e.g. Gibson and Ashby, 1997), a pure shear deformation in the finite strain regime causes not only non-vanishing shear stresses $\bar{\tau}_{12}$ but also significant normal stresses $\bar{\tau}_{11}$ and $\bar{\tau}_{22}$. The reason for this effect is the underlying microstructural mode of deformation. At large effective shear strains $\bar{\gamma}_{12}$, the cell walls are aligned into an inclined direction with an angle of 45° with respect to both, the x_1- and x_2-axes. Since this alignment is also associated with distinct stretching of the aligned cell walls into their longitudinal direction, non-vanishing normal stresses $\bar{\tau}_{11}$ and $\bar{\tau}_{22}$ develop (Hohe and Becker, 2003). This effect cannot be observed in small strain analyses since the re-orientation of the cell walls cannot properly be described under the assumption of small deformations.

Another specific feature which cannot be observed at small effective strains is the deformation-induced anisotropy which develops in terms of the normal stress components $\bar{\tau}_{11}$ and $\bar{\tau}_{22}$ in case of the pure shear deformation on the effective level. At small effective strains, the perfectly regular hexagonal microstructure with vanishing disorder ($\Delta x_1/l = 0$) is isotropic due to it's threefold symmetry (Christensen, 1987). Consequently, the effective stress components $\bar{\tau}^{a}_{11}$ and $\bar{\tau}^{a}_{22}$ are equal for this geometry if the effective strain is small or moderate ($\bar{\tau} \leqslant 0.1$). At larger effective strain levels, increasing differences between the two in-plane normal stress components are observed (see Fig. 7). The kink in the curve $\bar{\tau}_{22}(\bar{\gamma}_{12})$ which separates the decreasing part of the stress–strain curve from the secondary increase marks a bifurcation of the stress–strain curve due to a microstructural instability. Similar to the case of uniaxial compressive deformation, only the stable branch is presented in the postbuckling range.

In the probabilistic analyses, no bifurcation of the macroscopic mean stress $\bar{\tau}^{a}_{22}$ occurs. With increasing degrees $\Delta x_i/l$ of microstructural disorder, the stress strain curve $\bar{\tau}^{a}_{22}(\bar{\gamma}_{11})$ developes towards a curve which increases monotonically with the level of the effective strain $\bar{\gamma}_{11}$. Throughout the considered range of the effective shear strain $\bar{\gamma}_{12}$, the standard deviations $\bar{\tau}^{s}_{22}$ especially for large degrees $\Delta x_i/l$ of microstructural disorder are of the same order of magnitude as the corresponding mean values $\bar{\tau}^{a}_{22}$ indicating large scatter band widths. The same effect is observed in case of the second in-plane stress component $\bar{\tau}_{22}$ as well as in case of the shear stress component $\bar{\tau}_{12}$. In case of the effective shear strain it is observed that an increasing degree of microstructural disorder results in a softening of the microstructure with decreasing stress mean values $\bar{\tau}^{a}_{12}$ at high effective strain levels. For small effective strain levels, the opposite effect is observed. Due to the increasing disorder of the microstructure, the microstructural mode of deformation is shifted from pure bending in case of a perfectly regular microstructure and $\bar{\gamma}_{12} \to 0$ to a mode of deformation which consists of both, bending and stretching deformation on the cell wall level. This mode involves more strain energy than the pure bending mode and therefore results in higher effective stress levels. Nevertheless, it should be noted that due to the large scatter band widths indicated by standard deviations $\bar{\tau}^{s}_{12}$ which are in the same order of magnitude as the corresponding mean values $\bar{\tau}^{a}_{12}$ and (in some ranges) beyond, even an effective stress–strain response close to the curve corresponding to the perfectly periodic microstructure might occur with a non-negligible probability.

3.4. Effect of the material distribution along the cell walls

In all previous analyses, a constant material distribution with $t^c/t^i = 1$ along the cell walls has been assumed. For real foams, this fraction will be less than one. Therefore, the effect of the material distribution along the cell walls is studied in more detail. Two different macroscopic modes of deformation are considered:

- uniaxial tensile deformation with $\bar{\gamma}_{22} = \bar{\gamma}_{12} = 0$ and a prescribed nonvanishing effective strain $\bar{\gamma}_{11}$ at the levels of $\bar{\gamma}_{11} = 0.01$ as well as $\bar{\gamma}_{11} = 0.2$ and
- uniaxial compressive deformation with $\bar{\gamma}_{11} = -0.01$ and $\bar{\gamma}_{11} = -0.2$ where $\bar{\gamma}_{22} = \bar{\gamma}_{12} = 0$.

The ratio t^c/t^i is varied over the total possible interval from small values close to zero towards the case $t^c/t^i = 1$ where the cell wall thickness is constant along the individual struts. In all cases, the actual values of t^c and t^i are chosen according to the prescribed ratio in such a manner that the relative density of the foam $\bar{\rho} = 5\%$. The same degrees $\Delta x_i/l$ of microstructural disorder as in the previous analyses (see Section 3.3) are considered. The results are presented in Fig. 8.

For both tensile load cases, it is observed that for typical cell wall thickness ratios for standard foams ($t^c/t^i \in [0.5,1]$) the material distribution has nearly no effect on both, the stress $\bar{\tau}_{11}$ acting within the macroscopic loading direction as well as the net stress $\bar{\tau}_{22}$ perpendicular to the macroscopic loading direction. Therefore, the simplified assumption of uniform cell wall thickness, as it has been made in the previous investigations, is clearly justified in this range of the cell wall thickness ratio t^c/t^i. For smaller thickness ratios, as $t^c/t^i \to 0$, a progressive decrease of both stress components is observed. In this range, the deformation of the cell walls is increasingly localized in the vicinity of the centers of the individual cell walls whereas the cell wall deformation in the vicinity of the cell wall intersections decreases. The strain localization in

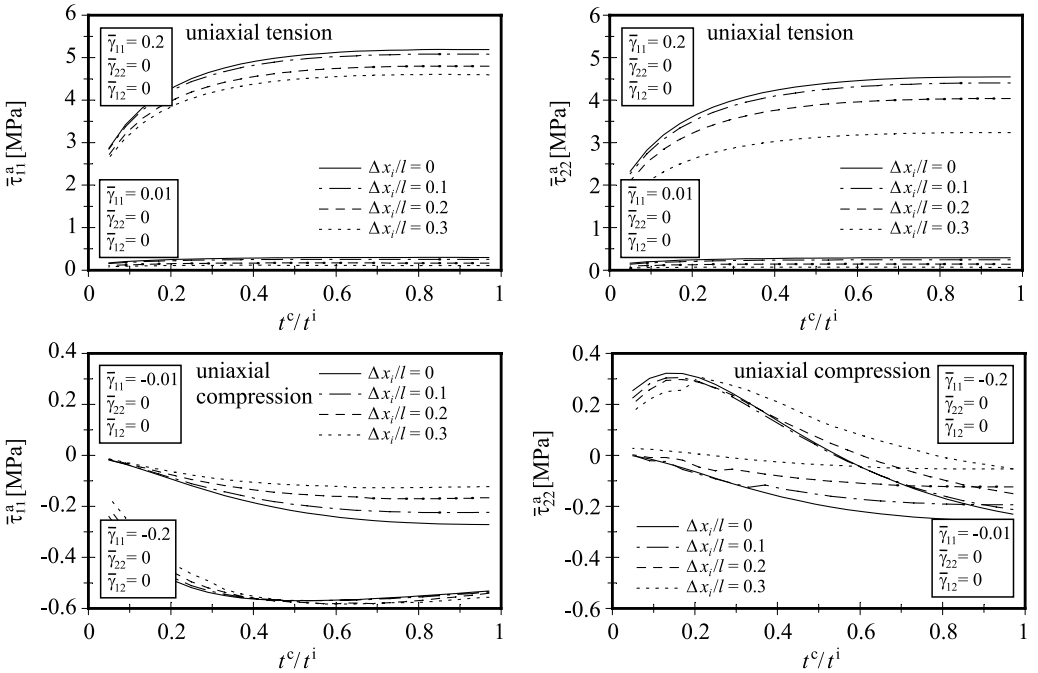

Fig. 8. Effect of the material distribution along the cell walls.

conjunction with the decreasing thickness at the cell wall centers causes the decrease of the effective stresses. Again, an increasing degree of microstructural disorder causes a general weakening of the structure on the macroscopic level.

Similar to the cases of uniaxial tensile deformation, only minor effects of the cell wall thickness ratio t^c/t^i on the stress component $\bar{\tau}^a_{11}$ are observed in the interval [0.5, 1] for uniaxial compressive deformation. For lower cell wall thickness ratios, a rapid decrease of the effective stress level is observed due to microscopic strain localization effects. At the low effective strain level $\bar{\gamma}_{11} = -0.01$ the effect of the degree $\Delta x_i/l$ of the microstructural disorder is more severe than in the tensile load cases. The effective stress level for the perfectly regular microstructure is approximately twice the effective stress level for the microstructure with the maximum microstructural disorder. This strong effect derives from the fact that the effective strain level of $\bar{\gamma}_{11} = -0.01$ is close to the bifurcation of the effective stress–strain curve of the perfectly periodic microstructure where strong effects of microstructural geometric imperfections have to be expected (see also Fig. 7). For the net stress $\bar{\tau}^a_{22}$, the effect of the cell wall thickness ratio t^c/t^i is stronger, especially for the large effective strain level ($\bar{\gamma}_{11} = -0.2$). The reason for this strong effect is a change in the microstructural mode of deformation in the postbuckling range for moderate and small t^c/t^i. For decreasing cell wall thickness ratios, the microstructural mode of deformation changes from distributed bending of the entire cell walls to localized bending around the center of the cell walls in conjunction with a rotation of the nearly undeformed areas around the cell wall intersections. Some scatter in the stress mean values for small cell wall thickness ratios is due to the shrinking database in this range since in a few cases of extreme microstructures, no numerical solution has been obtained.

3.5. Effect of the relative density

The most important microstructural property for amorphous foams is the relative density $\bar{\rho}$. The effect of this quantity is studied in the final parameter study. In this parameter study, the same effective loading conditions are considered as in the study concerning the effect of the cell wall material distribution (see Section 3.4). The material distribution along the struts is assumed to be uniform with $t^c = t^i$ again. The prescribed relative density is varied from 1% to 25%. The results are presented in Fig. 9 where the plots in the first two lines are directed to the in-plane normal stresses $\bar{\tau}^a_{11}$ and $\bar{\tau}^a_{22}$ for the two macroscopic strain levels in tension whereas the corresponding results for the two compressive load cases are presented in the last line.

For both uniaxial tensile deformation cases, an almost linear dependence of the effective stresses $\bar{\tau}^a_{11}$ and $\bar{\tau}^a_{22}$ on the relative density is obtained. This result indicates that the underlying micromechanical mode of deformation is dominated by cell wall stretching since the stretching stiffness of the cell walls increases linearly with the cell wall thickness $t^c = t^i$ which depends linearly on the relative density $\bar{\rho}$ of the foam. Thus, the microscopic mode of deformation consists of localized cell wall bending in the vicinity of the cell wall intersections to enable an alignment of the cell walls into the macroscopic loading direction whereas the aligned cell walls are deformed by stretching in their longitudinal direction. Since stretching deformation involves a much higher strain energy density than bending deformation, the stretching mode dominates the behavior of the foam on the effective level of structural hierarchy.

For small effective deformation levels ($\bar{\gamma}_{11} = 0.01$) the effect of the relative density on the effective stresses changes for increasing degrees $\Delta x_i/l$ of microstructural disorder. Especially for the model foam with the largest degree of microstructural disorder ($\Delta x_i/l = 0.3$), a distinct nonlinear increase especially of the stress mean value $\bar{\tau}^a_{11}$ within the loading direction is observed. This result indicates that the underlying microstructural mode of deformation changes from a stretching dominated mode to a mode dominated by cell wall bending. For larger amounts of effective deformation (see the results for $\bar{\gamma}_{11} = 0.2$), no such effect exists. Due to the large microstructural irregularity at $\Delta x_i/l = 0.3$, a bending dominated microstructural deformation is enabled at small levels of effective deformation until the cell walls are re-aligned in such a manner that any further deformation requires a significant amount of longitudinal stretching of the individual cell

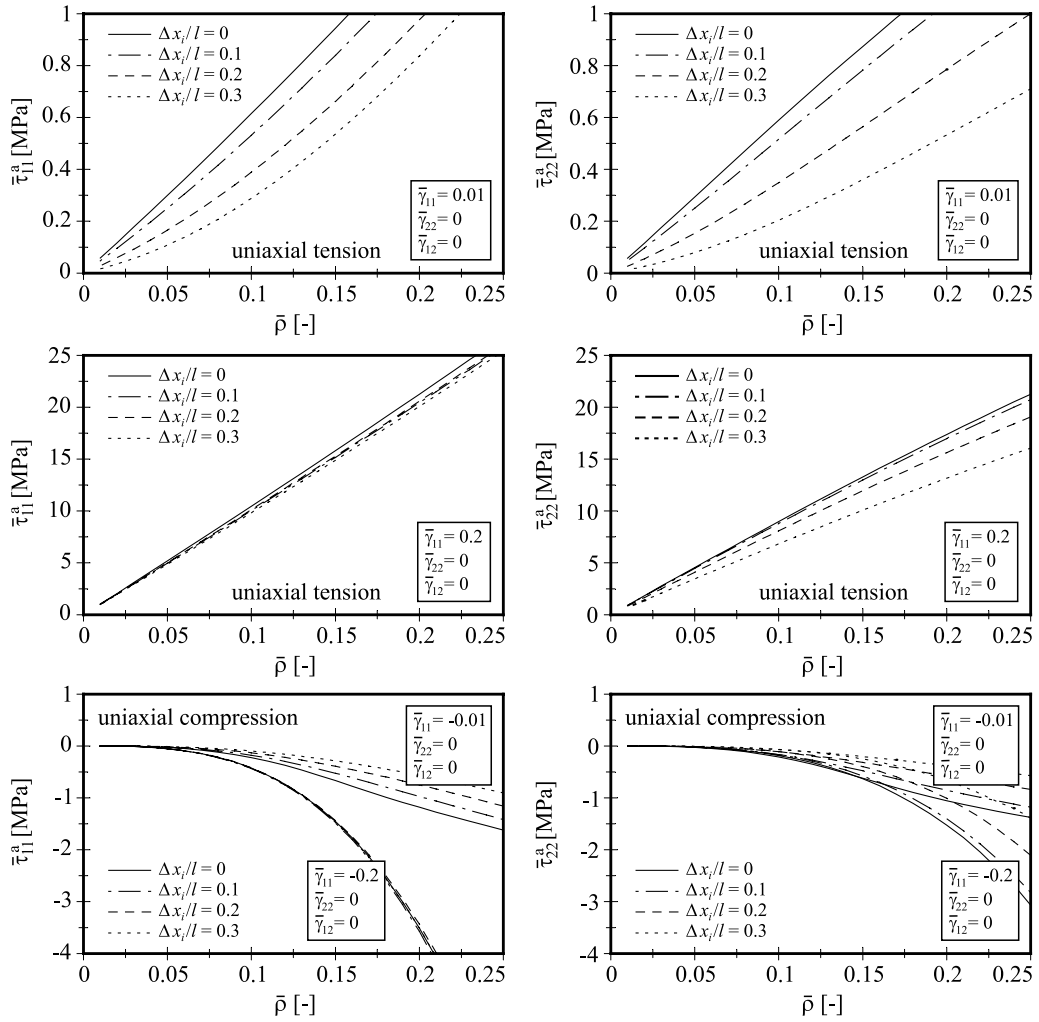

Fig. 9. Effect of the relative density.

walls. In this range of the effective deformation, the dependence of the effective stresses on the relative density becomes linear again.

Under uniaxial compressive deformation, an entirely different effect is observed (see the bottom two plots in Fig. 9). For high levels of compressive deformation ($\bar{\gamma}_{11} = -0.2$), the dependence of the effective stresses $\bar{\tau}^a_{ij}$ on the relative density $\bar{\rho}$ is nonlinear irrespectively of the degree $\Delta x_i/l$ of microstructural disorder. At this level of effective deformation, the perfectly regular hexagonal microstructure is in the postbuckling range where the microstructural mode of deformation consists in distributed bending of the (buckled) cell walls but involves nearly no longitudinal deformation of any of the cell walls in the representative volume element. The geometrically imperfect, disordered microstructures are deformed in a similar manner governed by cell wall bending so that the macroscopic stresses must depend in a nearly cubic manner on the relative density $\bar{\rho}$. At small levels of effective deformation ($\bar{\gamma}_{11} = -0.01$), a nonlinear characteristic of the stress vs. relative density curves is obtained only for small relative densities. Only in this range, the microstructure is in a postbuckling state. For large relative densities, the buckling load for the perfectly

regular structure is not exceeded due to the large cell wall thickness. Therefore, the dependence of the effective stresses $\bar{\tau}^{a}_{ij}$ on the relative density $\bar{\rho}$ is again linear in this range of the relative density. Since for the case $\bar{\gamma}_{11} = -0.01$ the load level is close to the bifurcation load of the perfectly regular hexagonal microstructure, a distinct softening of the structure is observed as the degree $\Delta x_i/l$ of microstructural disorder and therefore the geometric imperfection of the model foam increases.

4. Conclusion

The subject of the present study is the analysis of the effect of microstructural irregularity on the macroscopic stress–strain response of solid foams. For the homogenization analysis, a probabilistic approach is proposed which is based on the multiple analysis of a small-scale representative volume element with a randomized microstructure. In this context, the foam topology is prescribed whereas the spatial positions of the cell wall intersections are determined randomly within prescribed areas. The spatial extent of these areas forms an additional microstructural parameter defining the possible microstructural disorder. The results of the multiple homogenization analyses are evaluated by standard stochastic procedures.

Within this approach, a strain-energy based procedure is utilized for the homogenization of the microstructure. This scheme defines the macroscopic mechanical equivalence of a representative volume element for the cellular microstructure and a corresponding volume element consisting of the effective medium by the condition that the average strain energy density in both volume elements has to be equal, provided that the volume average of the deformation gradient is equal in both elements. Advantage of this approach is that Hill's principle is satisfied in a natural manner. No restrictions with respect to the geometry and topology of the microstructure apply. The scheme can be applied in both the infinitesimal and the finite strain regime. The effective stress and strain tensors are determined on the macroscopic level by means of their definitions in terms of the strain energy density and the deformation gradient. In this context, the study is restricted to hyperelastic materials.

The proposed probabilistic scheme forms a numerically efficient and reliable procedure. The additionally introduced microstructural parameter to define the degree of microstructural disorder can easily be determined for any given cellular solid from micrographic observations. Compared to the standard procedure of a single analysis of a large-scale representative volume element consisting of a large number of cells obtained by a Voronoi technique, the present approach has the advantage that the scatter of the effective material properties can be assessed in terms of the standard deviation which is not available in the standard procedure. Thus, predictions based on the present approach do not only give the mean value of the effective stresses to be expected for any given effective strain state but they may also give information about the scatter band within which the effective stresses have to be expected. Since representative volume elements consisting of rather small numbers of cells prove to be sufficient, the proposed probabilistic homogenization scheme can be applied in a numerically efficient manner.

Subsequently, the proposed scheme is applied to the numerical determination of the effective stress-strain response of two-dimensional cellular solids at finite strains. It is observed that at large tensile deformation, the effective material response is governed by an alignment of the cell walls into the macroscopic loading direction. At large compressive and shear deformation levels, microstructural instabilities cause material instabilities on the macroscopic level. Both effects cannot properly be addressed in small strain analyses. Other non-classical effects consist in deformation induced anisotropies of initially isotropic structures and deformation induced changes in the generalized effective Poisson's ratios of the material.

Regarding the effect of the microstructural disorder, it is observed that this property can have a variety of different effects. In general, an increasing degree of disorder on the microstructural level causes a decrease in the effective stiffness. Nevertheless, deep in the postbuckling range under compressive or shear deformation, the opposite effect might also occur. In this context, the point of occurrence of a negative effective

Poisson's ratio under compressive deformation is shifted towards significantly lower levels of the effective deformation, if the degree of microstructural disorder is increased. In all cases, an increasing degree of microstructural disorder causes a transition in the microstructural mode of deformation from a mode dominated by stretching of the individual cell walls into their longitudinal direction with only slight localized bending effects towards modes of deformation which involve much higher amounts of bending deformation on the microscopic level.

In general, increasing degrees of microstructural disorder result in increasing scatter of the effective stresses indicated by increasing standard deviations. Whereas the scatter band width under tensile deformation is small or moderate compared to the stress mean values, the standard deviation can be in the same order of magnitude as the corresponding mean value even for small degrees of microstructural disorder, if the foam is deformed in a compressive or shear mode on the effective level.

Thus, the microstructural disorder of amorphous solid foams has distinct effects on their effective stress–strain behavior. Analyses based on regular periodic foam models might yield inaccurate results even for the mean values of the effective stresses. For a more accurate analysis, probabilistic models should be utilized. In this context, the presently proposed model might be an efficient tool for a more reliable numerical homogenization analysis.

References

Ashby, M.F., 1983. The mechanical properties of cellular solids. Metallurgical Transactions 14A, 1755–1769.

Blazy, J.S., Marie-Louise, A., Forest, S., Chastel, Y., Pineau, A., Awade, A., Grolleron, C., Moussy, F., 2004. Deformation and fracture of aluminium foams under proportional and multi-axial loading: statistical analysis and size effect. International Journal of the Mechanical Sciences 46, 217–244.

Chen, C., Lu, T.J., Fleck, N.A., 1999. Effect of imperfection on the yielding of two-dimensional foams. Journal of the Mechanics and Physics of Solids 47, 2235–2272.

Christensen, R.M., 1986. Mechanics of low density materials. Journal of the Mechanics and Physics of Solids 34, 563–578.

Christensen, R.M., 1987. Sufficient symmetry conditions for isotropy of the elastic moduli tensor. Journal of Applied Mechanics 54, 772–777.

Cuitiño, A.M., Zheng, S., 2003. Taylor averaging on heterogeneous foams. Journal of Composite Materials 37, 701–713.

Dement'ev, A.G., Tarakanov, O.G., 1970. Effect of cellular structure on the mechanical properties of plastic foams. Polymer Mechanics 6, 519–525.

Fazekas, A., Dendievel, R., Salvo, L., Bréchet, Y., 2002. Effect of microstructural topology upon the stiffness and strength of 2D cellular structures. International Journal of the Mechanical Sciences 44, 2047–2066.

Fortes, M.A., Ashby, M.F., 1999. The effect of non-uniformity on the in-plane modulus of honeycombs. Acta Materialia 47, 3469–3473.

Gent, A.N., Thomas, A.G., 1963. Mechanics of foamed elastic materials. Rubber Chemistry and Technology 36, 597–610.

Gibson, L.J., 1989. Modelling the mechanical behavior of cellular materials. Materials Science and Engineering A 110, 1–36.

Gibson, L.J., Ashby, M.F., 1997. Cellular Solids—Structure and Properties. Cambridge University Press, London.

Grenestedt, J.L., Bassinet, F., 2000. Influence of cell wall thickness variations on elastic stiffness of closed-cell cellular solids. International Journal of the Mechanical Sciences 42, 1327–1338.

Hall, R., 1993. Effective moduli of cellular materials. Journal of Reinforced Plastics and Composites 12, 186–197.

Hohe, J., Becker, W., 2001a. An energetic homogenization procedure for the elastic properties of general cellular sandwich cores. Composites Part B 32, 185–197.

Hohe, J., Becker, W., 2001b. A refined analysis of the effective elasticity tensor for general cellular sandwich cores. International Journal of Solids and Structures 38, 3673–3687.

Hohe, J., Becker, W., 2002. Effective stress–strain relations for two-dimensional cellular sandwich cores: Homogenization, material models and properties. Applied Mechanics Reviews 55, 61–87.

Hohe, J., Becker, W., 2003. Effective mechanical behavior of hyperelastic honeycombs and two-dimensional model foams at finite strain. International Journal of the Mechanical Sciences 45, 891–913.

Huyse, L., Maes, M.A., 2001. Random field modeling of elastic properties using homogenization. Journal of Engineering Mechanics 127, 27–36.

Kraynik, A.M., Reinelt, D.A., Princen, H.M., 1991. The nonlinear elastic behavior of polydisperse hexagonal foams and concentrated emulsions. Journal of Rheology 35, 1235–1253.

Lakes, R., 1993. Materials with structural hierarchy. Nature 361, 511–515.
Ogden, R.W., 1984. Non-Linear Elastic Deformations. Ellis Horwood Ltd, Chichester.
Patel, M.R., Finnie, I., 1970. Structural features and mechanical properties of rigid cellular plastics. Journal of Materials 5, 909–932.
Ramamurty, U., Paul, A., 2004. Variability in mechanical properties of a metal foam. Acta Materialia 52, 869–876.
Roberts, A.P., Garboczi, E.J., 2001. Elastic moduli of model random three-dimensional closed-cell cellular solids. Acta Materialia 49, 189–197.
Silva, M.J., Hayes, W.C., Gibson, L.J., 1995. The effects of non-periodic microstructure on the elastic properties of two-dimensional cellular solids. International Journal of the Mechanical Sciences 37, 1161–1177.
Thomson, W. (Lord Kelvin), 1887. On the division of space with minimum partitional area. Philosophical Magazine 24, 503–514.
van der Burg, M.W.D., Shulmeister, V., van der Giessen, E., Marissen, R., 1997. On the linear elastic properties of regular and random open-cell foam models. Journal of Cellular Plastics 33, 31–54.
Warren, W.E., Kraynik, A.M., 1988. Foam mechanics: the linear elastic properties of open-cell foams. Journal of Applied Mechanics 55, 341–346.
Warren, W.E., Kraynik, A.M., 1997. Linear elastic behavior of a low-density Kelvin foam with open cells. Journal of Applied Mechanics 64, 787–794.
Zohdi, T.I., Wriggers, P., 2001. Aspects of the computational testing of the mechanical properties of microheterogeneous material samples. International Journal for Numerical Methods in Engineering 50, 2573–2599.
Zhu, H.X., Hobdell, J.R., Windle, A.H., 2001. Effects of cell irregularity on the elastic properties of 2D Voronoi honeycombs. Journal of the Mechanics and Physics of Solids 49, 857–870.